Journal of Biodiversity and Environmental Sciences (JBES)
ISSN: 2220-6663 (Print) 2222-3045 (Online)
Vol. 8, No. 1, p. 52-64, 2016
http://www.innspub.net

INNSPUB
RESEARCH PAPER
OPEN ACCESS

Zircon U–Pb geochronology, geochemistry, petrogenesis and tectonic significance of the boroon igneous masses (East of Iran)

Saied Ansari[1*], Mina Sakhdari[1]

Department of Geology, Ferdowsi University of Mashhad, Iran

Article published on January 10, 2016

Key words: Petrogenesis, Magmatic evolution, Boroon, Lut block, Iran.

Abstract

The Boroon igneous masses are Cu bearing porphyries that outcrop in the North part of the Lut Block, about 20 km north-west of Ferdows. These igneous masses occur mainly as dykes and stocks that intrude Eocene volcanics and pyroclastics. Hydrothermal alteration affected these igneous masses, as revealed by the common ocurrence of sericite, chlorite, sphene/leucoxene, epidote and calcite. Chemical classification criteria show that the intrusives may be named as gabbrodiorites, diorites, monzodiorites and tonalites. Major element geochemistry reveals that all the studied lithologies are typically metaluminous (A/CNK ≤ 0.9) and, in addition, trace element patterns normalized to chondrite and primitive mantle are very similar to each other and show enrichments in LREE relative to HREE and in LILE relative to HFSE, as well as negative anomalies of Ta, Nb and Ti. Eu/Eu* ratios vary from 0.88 (in the most mafic composition) to 0.65, showing that plagioclase played a role in magma differentiation. LA-MC-ICP-MS U-Pb zircon data from Tonalite Porphyry yield similar concordia ages of ca. 40.31±1.1 Ma (2σ), which corresponds to the Eocene period. The whole set of geochemical data agree with the emplacement of the studied intrusions in a magmatic belt above a subduction zone. Primitive magmas should have formed by melting of mantle wedge peridotite, and, during magma ascent to crustal levels, both magma differentiations by crystal fractionation and crustal contamination took place. Sulfide mineralizations related to these igneous masses is common and occurs both disseminated and as hydrothermal veins, indicating a high mineralization potential for this area.

***Corresponding Author:** Saied Ansari ✉ Saied.Ansari@Yahoo.com

Introduction

More than forty years ago Lut block was introduced by Stocklin (1968) in the east of Iran and over the last three decades, studies on the geology, petrology, geochemistry and geochronology of Lut block have revealed diverse hypotheses types about formation (Camp and Griffis, 1982; Tirrul *et al.,* 1983*;* Arjmandzadeh *et al.,* 2011*;* Pang *et al,* 2013). The geology of Lut block is characterized by occurrence of widespread Tertiary granitoides and volcanic rocks, which are rich in mineral resources such as W, Sn, Au, Cu, Pb, Zn and REE. The Lut block has N–S direction (Fig. 1). There is complex tectonic history about genesis of these rocks. New geochronology studies of Zircon U\Pb dating indicate that the generation of oceanic lithosphere was still active in the Middle Cretaceous (Zarrinkoub *et al.,* 2012). The mechanism and timing of ocean closure remains poorly understood. For example, models involving eastward subduction beneath the Afghan block (Camp and Griffis, 1982; Tirrul *et al.,* 1983), western subduction beneath the Lut block (Zarrinkoub *et al.,* 2012), two-sided subduction (Arjmandzadeh *et al.,* 2011) , eastward intraoceanic subduction (Saccani *et al.,* 2010*)* and last hypothesisis is that the magmatism was triggered by convective removal of the lithosphere and resultant asthenospheric upwelling during extensional collapse of the east Iranian ranges in the Eocene–Oligocene (Pang *et al,* 2013). The age for ocean closure and thus the Lut–Afghan collision was considered by some workers to occur in the Middle Eocene (Camp and Griffis, 1982; Tirrul *et al.,* 1983) or by others in the Late Cretaceous (Angiboust *et al.,* 2013). The study area, called the Boroon prospecting area, located in the center of the Lut block, eastern Iran (Fig. 1). The Boroon prospecting area is an epitermal Cu-Zn mineralization (Mirzaee *et al,* 2012) that there was no information on the absolute age and relation of various intrusions with mineralization. The area contains various intrusive rocks, such as dykes and stocks, which intruded into older pyroclastic and volcanic units. The purpose of this work is to present and discuss new Geochemical (both elemental and isotopic) and geochronological (U–Pb) data, aiming at establishing tighter constraints to the petrogenetic processes and the geodynamic evolution of the granitoids of the Boroon prospecting area.

Materials and methods

Fresh rock samples were prepared in three groups: thin sections for petrography; 200 micron mesh powder for major, trace element, and Sr–Nd isotope analyses; and 40–60 micron mesh crushings for zircon separation and U–Pb dating.

Major and trace element analysis

The present study involved detailed field work and petrographic study of more than 100 samples of intrusive, volcanic and pyroclastic rocks from the Boroon prospecting area. Seventeen samples were analyzed for major elements by wave-length-dispersive X-ray fluorescence (XRF) spectrometry using fused disks and the Philips PW 1410 XRF spectrometer at East Amytis Company, Mashhad, Iran. Thirteen of these samples were analyzed for trace elements using inductively coupled plasma–mass spectrometry (ICP-MS), following a lithium metaborate/tetraborate fusion and nitric acid total digestion.

Two samples (367 and M15) from outcrops of the sub volcanic and intrusive from the Boroon prospecting area were collected for LA-ICP-MC–MS zircon U–Pb analyses. The LA-ICP-MC–MS analytical work was performed at the Laboratory of Geochronology, Center for Earth Sciences, University of Vienna. They were separated by heavy liquid and magnetic separation, followed by hand picking under a binocular microscope. More than 80 zircon grains from each sample were found. The sizes of the zircons are 100–200 μm in length and 30–100 μm in width. The handpicked inclusion free zircon fractions were mounted in epoxy and then ground and polished prior to CL imaging and LA-ICP-MC–MS analysis.

CL imaging was performed with a TESCAN CL DECTOR SEM with 15 kV acceleration voltages at

GOELOGICAL SURVEY OF VIENNA, AUSTRIA. Cathodoluminescence (CL) images were obtained before LA-ICP-MC–MS dating of the zircon crystals in order to distinguish between different zircon domains. The imaging was repeated after the LA-ICP-MC–MS measurements to confirm the exact location of the spots/line paths.

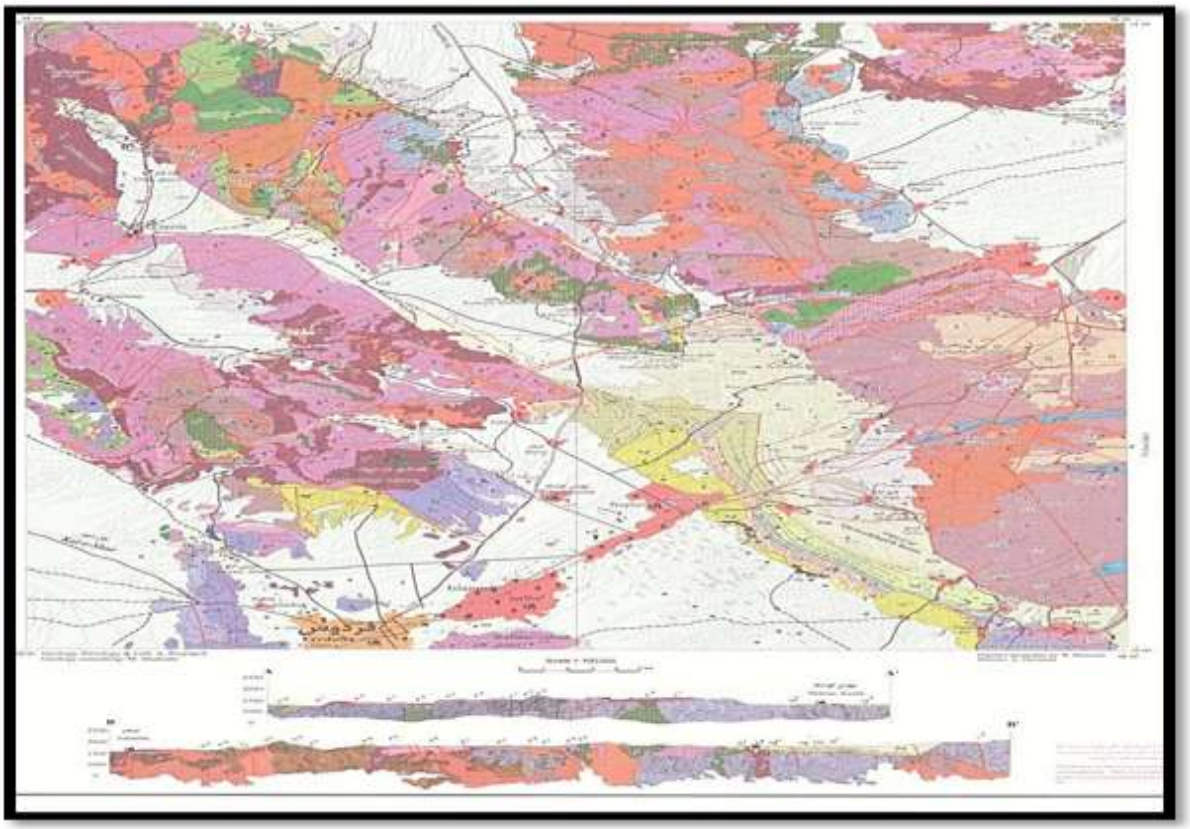

Fig. 1. 1:250000 Geological map of Ferdows.

Results and discussion

The Boroon prospecting area is in the Tertiary metallogenic volcano-plutonic belt of the Lut block. Geology of the Lut block mainly includes Cenozoic silicic to mafic volcanic rocks, which have been intruded by granitoid units of granitic to dioritic composition.The geological units are: Paleocene-Eocene volcanic and pyroclastic rocks which were intruded telescopically by several sub volcanic and intrusive bodies. Eocene sub volcanic bodies which are altered with different degrees.Oligocene intrusive body .young alluvium terraces, clay flat, sand dome and recent alluvium belong to Quaternary. The volcanic and plutonic rocks of the district according to the map compilation belong to Eocene–Oligocene magmatic zone, which cross cuts older tectonic structures and occur within the Lut block. The middle Eocene to Early Oligocene intrusions in Lut block is partly associated with economic and non-economic ore mineralization (Karimpour *et al,* 2011).

The Boroon mineralization was introduced epitermal vein mineralization (Mirzaee *et al,* 2012) and mineralization is as disseminated and hydrothermal vein related to monzonite to quartz diorite porphyry (Miri *et al, 2013*). It was discovered in 2007 and detailed exploration Continued right now.

According to petrographic studies on the Boroon area comprises outcrops of Eocene volcanics and pyroclastics, which were intruded telescopically by several subvolcanic intermediate bodies such as hornblende diorite to quartz monzonite porphyry (Fig 2).

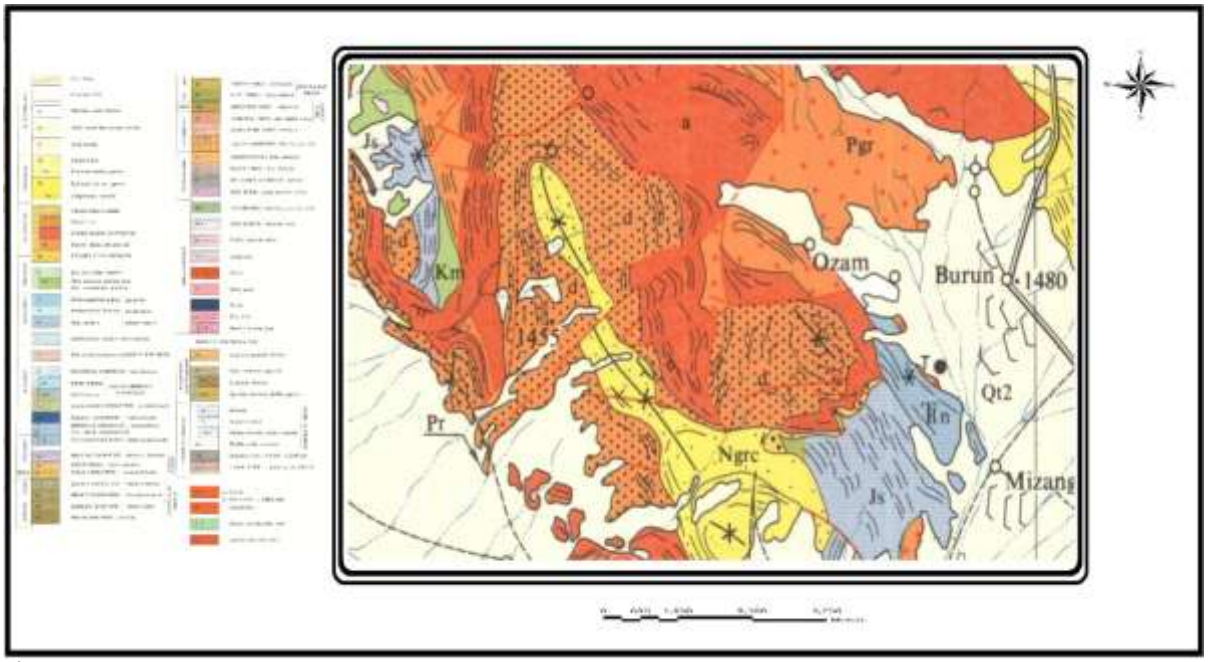

Fig. 2. Geological map of Boroon prospecting area.

Volcanic and pyroclastic rocks

Volcanic rocks in Boroon are Eocene tuff, lithic tuff, andesitic basalt, andesite, and dacite which are highly altered in central parts of the area. According to Rb–Sr dating, the andesitic basalt and andesite have a 33.5 ± 2 Ma age (Kluyver *et al.,* 1978).

Sub volcanic stocks

According to petrographic studies these bodies are composed of hornblende diorite porphyry, quartz diorite porphyry, hornblende quartz monzodiorite porphyry and hornblende quartz monzonite porphyry (Fig. 2). These are the main sub volcanic in the area which intruded into volcanic and pyroclastic rocks and occur mainly as dykes and small stocks. According to Zircon U\Pb dating in this study, the subvolcanic rocks have a 40.31 ± 0.82 Ma age. These rocks have porphyritic textures, characterized by abundant euhedral to subhedral phenocrysts of plagioclase and hornblende, and also some pyroxene. The same minerals, accompanied by anhedral quartz, are also present in the groundmass. Hydrothermal alteration is often observed by the presence of sericite, chlorite, calcite and epidote.

Table 1. Major (wt. %) and trace elements (ppm) data for the Boroon Granotoide rocks.

Sample No	M1	M2	M3	M4	M5	M6	M7	M8	M9
Rock type	D	D	Gd	Anb	Anb	Tph	An	An	Tph
Major elements**(%)**									
SiO2	57.73	58.25	55.83	54.96	56.17	63.74	57.95	56.98	60.90
TiO2	0.82	0.84	0.87	0.92	0.89	0.68	0.75	0.77	0.7
Al_2O_3	15.65	15.54	15.61	16.37	16.37	14.6	16.14	16	14.44
FeOt	7.42	7.4	7.91	8.33	7.8	5.56	7.56	7.43	6.29
MnO	0.17	0.15	0.17	0.16	0.19	0.11	0.18	0.15	0.12
MgO	4.28	4.11	4.59	3.69	4.36	3.16	5.35	4.88	3.04
CaO	6.13	6.35	7.5	7.82	7.31	3.21	6.08	6.36	4.26
Na_2O	3.42	3.18	2.9	3.38	3.01	3.46	2.89	2.86	3.68
K_2O	2.44	2.47	2.24	3.04	2.6	3.74	1.41	1.67	3.16
P_2O_5	0.3	0.32	0.3	0.24	0.24	0.19	0.28	0.27	0.24
LOI	1.64	1.52	1.27	0.41	0.8	1.3	2.17	2.15	1.92
SO_3	0	0	0	0	0	0	0	0	0
Na_2O/K_2O	1.4	1.29	1.29	1.39	1.16	0.92	2.05	1.71	1.16
Total	99.77	99.77	99.79	99.75	99.75	99.79	99.76	99.76	99.78
Trace elements (ppm**)**									

Ba	-	378	339	439	-	461	-	456	465
Hf	-	3.5	2.8	3.8	-	6	-	3.3	5
Ta	-	0.4	0.4	0.4	-	0.9	-	0.5	0.8
Cs	-	1.7	1.6	4.7	-	3.6	-	8.2	1.6
Co	-	15.8	19.4	21.7	-	11.7	-	16.9	11.5
Nb	-	7.6	6.9	6.7	-	10.9	-	8.8	9.3
Ce	-	41.1	37	38	-	59.1	-	48.4	49.6
Sr	-	397.2	454	428.4	-	326.6	-	581	412.3
Rb	-	63.1	51	76.3	-	154.3	-	74.4	82.3
Zr	-	133.4	121.5	115.8	-	220	-	140.7	171.4
La	-	20.1	17.3	18.2	-	29	-	25.4	24.9
Pr	-	4.89	4.61	4.56	-	6.5	-	5.67	5.84
Nd	-	20.1	17.3	19.4	-	23.6	-	20.4	22.8
Sm	-	4.13	4.35	4.22	-	5.12	-	4.39	4.63
Eu	-	1.13	1.11	1.17	-	1.03	-	1.08	1.11
Gd	-	4.35	4.51	4.39	-	4.55	-	4.06	4.67
Tb	-	0.64	0.61	0.66	-	0.64	-	0.61	0.66
Dy	-	3.7	3.94	4.05	-	4.65	-	3.66	4.39
Ho	-	0.83	0.72	0.83	-	0.84	-	0.74	0.84
Er	-	2.54	2.24	2.41	-	2.6	-	2.16	**2.42**
Tm	-	0.34	0.32	0.36	-	0.34	-	0.31	0.38
Yb	-	2.04	2.2	2.37	-	2.58	-	2.04	2.49
Lu	-	0.33	0.32	0.34	-	0.37	-	0.28	0.38
Y	-	23.5	23.5	22.5	-	24.1	-	20.7	26.9
Co	-	15.8	19.4	21.7	-	11.7	-	16.9	11.5
Th	-	4.9	5.4	5.2	-	14.3	-	7	9.4
U	-	1	1.2	1.3	-	3.3	-	1.6	1.9
Eu/Eu*	-	0.82	0.77	0.83	-	0.65	-	0.78	0.73
$(La/Yb)_N$	-	6.64	5.3	5.18	-	7.58	-	8.39	6.74
$(Yb)_N$	-	9.8	10.5	11.3	-	12.3	-	9.8	11.3

Table 2. (continued)

Sample No	M10	M13	M14	M15	M16	M18	M19	M21
Rock type	Tph	Dph	Mzdph	Tph	Gd	Dph	Tph	Gdph
Major elements**(%)**								
SiO2	63.88	59.8	59.18	63.44	56.37	60.28	64.34	51.65
TiO2	0.63	0.74	0.69	0.6	0.86	0.72	0.64	1.21
Al2O3	14.46	14.92	14.85	14.77	15.59	14.6	14.91	15.45
FeOt	5.39	6.49	7.02	5.48	7.81	6.62	3.76	9.52
MnO	0.11	0.11	0.13	0.11	0.16	0.12	0.05	0.2
MgO	2.62	4.57	4.64	2.66	4.98	4.28	2.64	**4.8**
CaO	3.47	4.18	4.11	3.63	7.42	4.67	4.19	6.99
Na2O	3.74	3.35	3.64	3.14	2.75	2.93	4.92	2.78
K2O	3.39	3.2	3.18	3.75	2.22	3.52	3.38	2.42
P2O5	0.2	0.25	0.28	0.27	0.31	0.22	0.24	0.49
LOI	1.52	2.16	2.06	1.87	1.32	1.83	0.61	4.29
SO3	0.34	0	0	0	0	0	0.06	0
Na_2O/K_2O	1.10	1.05	1.14	0.84	1.24	0.83	1.46	1.15
Total	99.75	99.77	99.78	99.72	99.79	99.79	99.74	99.8
Trace elements (ppm**)**								
Ba	496	387	430	520	-	442	483	310
Hf	4.9	4.5	4.2	4.4	-	5.4	5.5	3.3
Ta	0.8	0.7	0.9	0.7	-	0.6	0.8	0.5
Cs	2.2	3.7	5.3	2.6	-	5.2	1.8	5.4
Co	9.5	15.7	14.4	10.2	-	13.6	6.1	17.9
Nb	9.9	9.8	9.8	8.4	-	9.7	10.3	8.8

Ce	52.6	50.5	55.4	50.8	-	49	51	48.6
Sr	368	428.5	388.4	422.7	-	378	260.9	434.8
Rb	107.7	116.4	124.9	106.6	-	128.9	76.1	63.3
Zr	181.1	178	175.2	159.2	-	176.3	185.5	125.8
La	25.9	24.9	25.4	25.2	-	24.9	26	22.6
Pr	6	5.59	5.82	5.63	-	5.77	5.87	6.04
Nd	22	22.1	21.4	23.1	-	22.1	23	24.3
Sm	4.53	4.51	4.14	4.34	-	4.47	4.41	5.48
Eu	1.19	0.97	1	1.06	-	1.13	1.05	1.6
Gd	4.46	4.21	4.17	4.3	-	4.25	4.44	5.66
Tb	0.66	0.58	0.61	0.59	-	0.6	0.72	0.82
Dy	4.28	4.37	4.38	3.74	-	4	4.4	5.42
Ho	0.8	0.77	0.67	0.75	-	0.74	0.8	1.12
Er	2.64	2.24	2.02	2.01	-	2.19	2.53	2.94
Tm	0.37	0.34	0.33	0.32	-	0.33	0.39	0.44
Yb	2.83	2.07	2.19	2.18	-	2.09	2.7	3.13
Lu	0.36	0.37	0.35	0.33	-	0.34	0.39	0.45
Y	21	21.3	22.6	21.4	-	22.9	25.9	26.7
Co	9.5	15.7	14.4	10.2	-	13.6	6.1	17.9
Th	9.8	10.3	10.6	8.8	-	10.7	11.5	5.8
U	2.3	2.6	2.5	2.1	-	2.8	2.9	1.1
Eu/Eu*	0.81	0.68	0.74	0.75	-	0.79	0.73	0.88
$(La/Yb)_N$	6.17	8.11	7.82	7.79	-	8.03	6.49	4.87
$(Yb)_N$	13.5	9.9	10.5	10.4	-	10	12.9	15

(D)Diorite, (Gd)Gabrodiorite, (Dph)Diorite Porphyry, (Tph) Tonalite Porphyry, (Gdph)Gabrodiorite Porphyry, (Mzdph) Monzodiorite Porphyry, (Anb) Andesibasalte, (An) Andesite.

Zircon $^{206}Pb/^{238}U$ and 207Pb/206Pb ages were determined using a 193 nm solid state Nd-YAG laser (NewWave UP193-SS) coupled to a multi-collector ICP-MS (NuInstruments HR) at the University of Vienna. Ablation in a He atmosphere was either spot or raster wise according to the CL zonation pattern of the zircons. Spot analyses were 15–25µm in diameter whereas line widths for rastering were 10–15 µm with a rastering speed of 5 µm/s. Energy densities were 5–8J/cm² with a repetition rate of 10 Hz. The He carrier gas was mixed with the Ar carrier gas flow prior to the plasma torch. Ablation duration was 60 to 120 s with a 30 s gas and Hg blank count rate measurement preceding ablation. Ablation count rates were corrected accordingly offline. Remaining counts on mass 204 were interpreted as representing Pb^{204}. Static mass spectrometer analysis was as follows: U^{238} in a Faraday detector, Pb^{207}, Pb^{206}, and 204 (Pb+Hg) were in ion counter detectors. Pb^{208} was not analysed. An integration time of 1 s was used for all measurements. The ion counter Faraday and inter-ion counter gain factors were determined before the analytical session using standard zircons 91500 (Wiedenbeck *et al.*1995) and Plesovice (Slama *et al.* 2006). Sensitivity for ^{206}Pb on standard zircon 91500 was c. 30'000cps per ppm Pb. For U^{238} the corresponding value was c. 35'000.

Mass and elemental bias and mass spectrometer drift of both U/Pb and Pb/Pb ratios, respectively, were corrected using a multi-step approach: first-order mass bias is corrected using a desolvated $U^{233-205}$ Tl-203Tl spike solution which is aspirated continuously in Ar and mixed to the He carrier gas coming from the laser before entering the plasma. This corrects for bias effects stemming from the mass spectrometer. The strongly time-dependent elemental fractionation coming from the ablation process itself is then corrected for using the "intercept method"of Sylvester and Ghaderi (1997). The calculated Pb^{206}/U^{238} and Pb^{207}/Pb^{206} intercept values are corrected for mass discrimination from analyses of standards 91500 and Plesovice measured during the analytical session using a standard bracketing method. The correction

utilizes regression of standard measurements by a quadratic function. A common Pb correction was applied to the final data using the apparent $^{207}Pb/^{206}Pb$ age and the Stacey and Kramers (1975) Pb evolution model. The final U/Pb ages were calculated at 2σ standard deviation using the Isoplot/Ex program - version 3.00 (Ludwig, 2003).

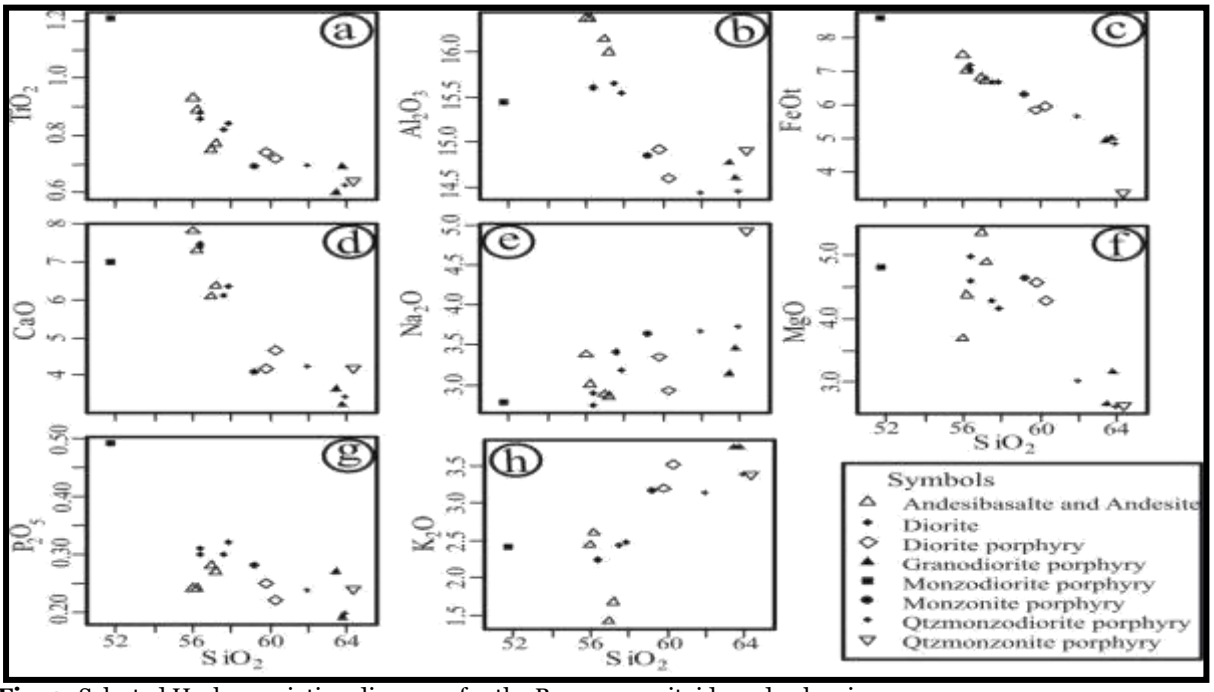

Fig. 3. Selected Harker variation diagrams for the Boroon granitoids and volcanic.

Major and trace elemental compositions for the rocks from the Boroon area are listed in Table 1. Harker diagrams show the variation of certain selected major elements as a function of SiO_2 content (Fig. 3). With increasing silica, MgO, FeO_t, Al_2O_3, P_2O_5, CaO and TiO_2 decreased, and K_2O increased. Rocks from the Boroon area have a relatively wide range of SiO_2 (52–64 wt.%). They have relatively high Na_2O (2.7–4.9 wt.%) and K_2O (1.4–3.8 wt.%), with high total alkali concentrations (K_2O+Na_2O=4.5–8.3wt.%) and K_2O/Na_2O ratios (0.69–1.2), high contents of CaO (3.21–7.82 wt.%) and FeO_t (3.76–9.52 wt.%), MgO (2.62–4.88wt.%), TiO_2 (0.6–1.21 wt.%), MnO (0.05–0.2 wt.%) and P_2O_5(0.19–0.49 wt.%). Al_2O_3 contents range from 14.4 to 16.4 wt.%. All granitoid samples plot in the fields of Gabrodiorite, Diorite, Monzodiorite and Tonalite of the Dela Roche *et al* (1980) diagram (Fig. 4a), and fall into the high-K calc-alkaline series field in the SiO_2 vs. K_2O diagram (Fig. 4b). All the calculated A/CNK values (molar Al_2O_3/ ($CaO+Na_2O+K_2O$)) are concentrated in the range from 0.7 to 0.95, indicating that these rocks are metaluminous (Fig. 5).

The Boroon granitoids have a large variation of trace elemental content (Table 1). In primitive mantle-normalized spidergrams (Fig. 6), all the samples exhibit similar trace elemental patterns, with significant negative anomalies of high field strength elements (HFSE, e.g., Nb, Ti and Zr) and P. There are positive anomalies of large ion lithophile elements (LILE, e.g., Rb, Th, Ba and U). In addition, compared to Rb and Th, Ba has significantly negative anomalies. The Boroon granitoids have similar chondrite-normalized REE profiles (Fig.7), The ∑REE ranges from 96.5 to 140.9 ppm, with LREE/HREE = 5.4–7.9 with weak to moderate enrichment of light REE [$(La/Yb)_N$=4.87–8.39] and a relatively flat heavy REE profile [$(Gd/Yb)_N$=1.33–1.72]. All of the rocks have weak negative Eu anomalies, with Eu/Eu* of 0.65 to 0.88.

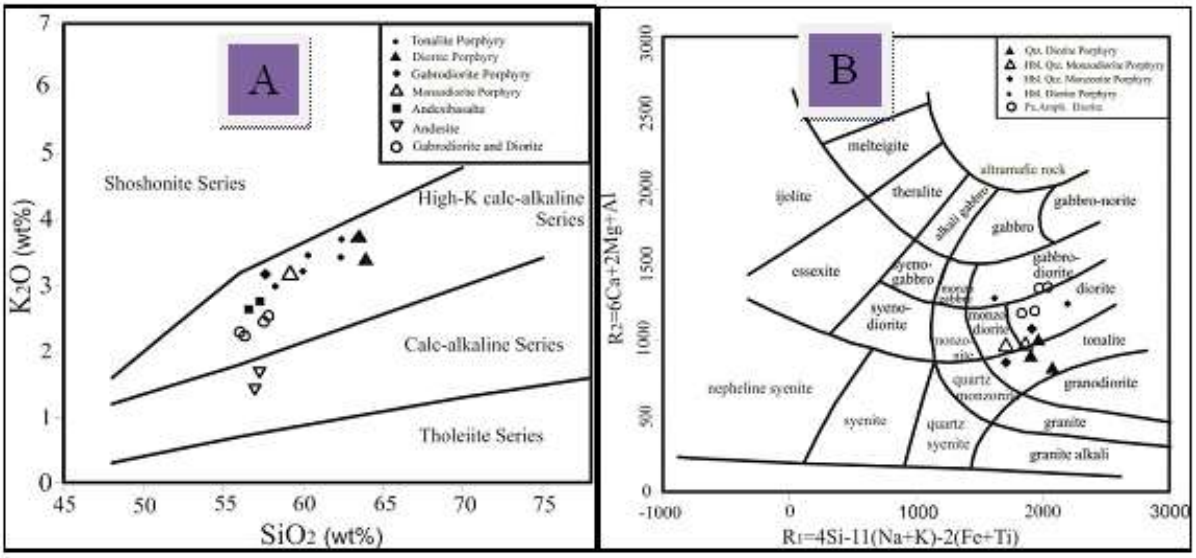

Fig. 4. (A) R1versus R2 and (B) SiO_2 versus K_2O diagrams for Boroon magmatic rocks. The field boundaries in (A) are from (Dela Roche *et al*, 1980) and in (B) are Peccerillo and Taylor (1976).

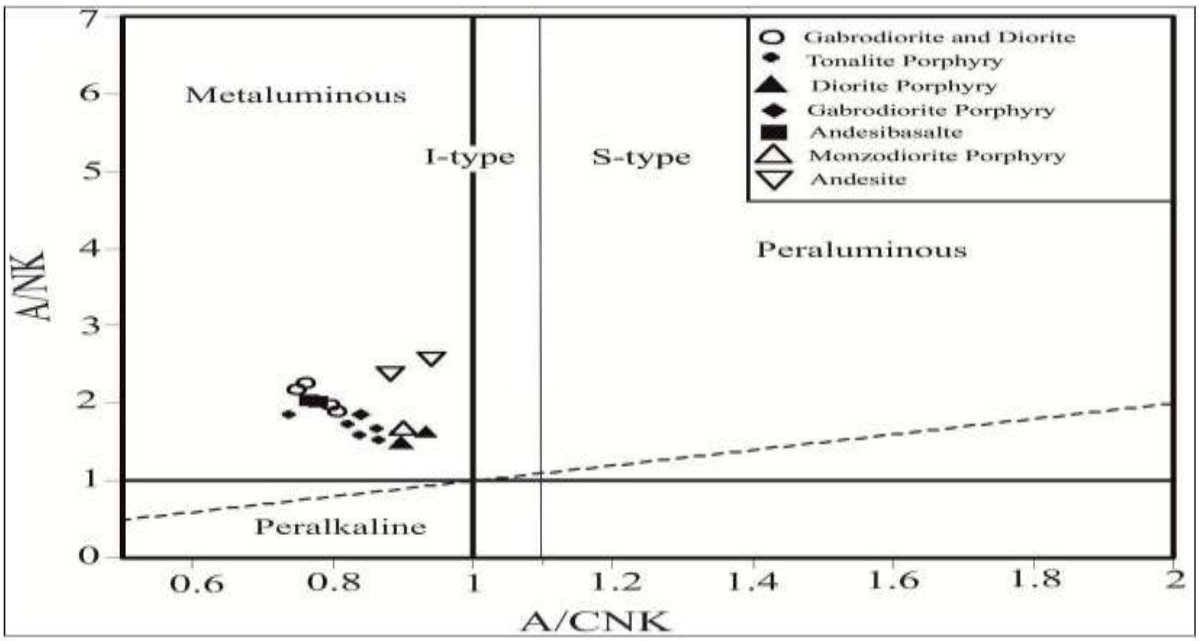

Fig. 5. Al_2O_3/Na_2O+K_2O (molar) vs. $Al_2O_3/(CaO + K_2O+Na_2O)$ (molar) (Maniar and Piccoli, 1989) and The field boundaries between S-type and I-type granite are from Chappell and White, 1992.

Zircon U–Pb results

Zircon CL images of the Boroon granitoids are shown in Fig. 8a and 8b. Most zircons have euhedral crystals that exhibit oscillatory zoning without distinctively older cores or younger overgrowths, suggesting their igneous origin (Hanchar and Hoskin, 2003). Twenty zircons of high transparency and free of visible inclusions were chosen for LA-ICP-MS U–Pb isotope analysis. U–Pb data are listed in Table 2. Measured U concentrations vary from 1 to 3.3 ppm, and Th ranges from 5.8 to 14.3 ppm, with Th/U ratios between 3.8 and 5.3. Excluding the two ages of 31.88 ± 0.2 Ma (367) and 40.31 ± 0.82 Ma (M15), the calculated weighted mean age accommodating the 6 remaining analyses is 31.88 ± 0.2 Ma (95% confidence) with an MSWD of 1.5 (Fig. 9A) for 367 sample and 40.31 ± 0.82 Ma (95% confidence) with an MSWD of 15 (Fig. 9B) for M15 sample.

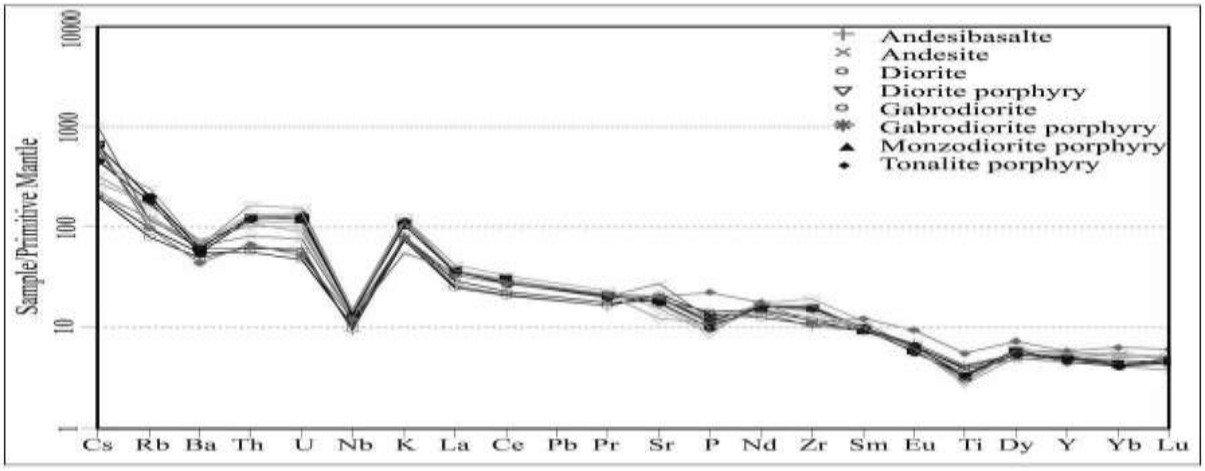

Fig. 6. Primitive-mantle-normalized trace element patterns .Normalizing values are from Sun and Mc Donough(1989).

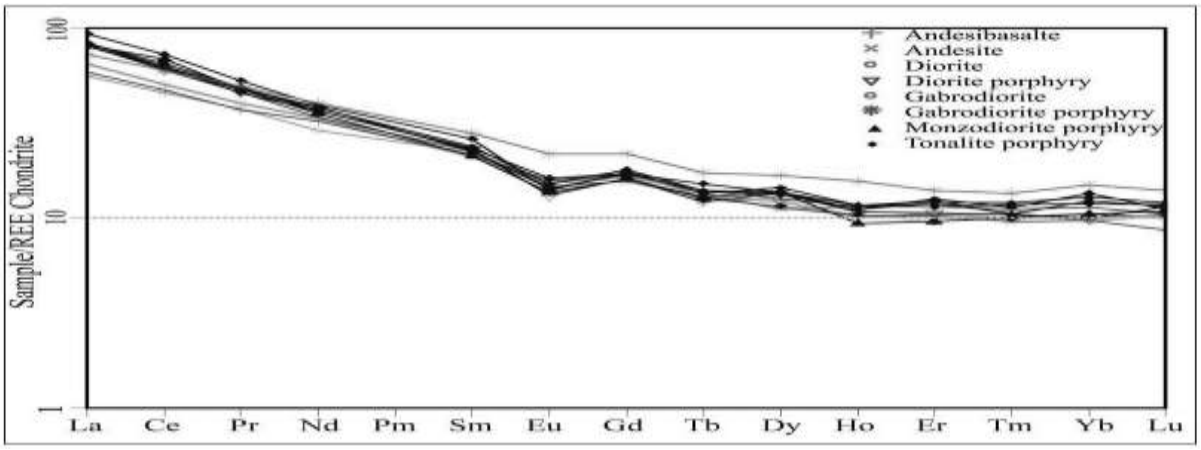

Fig. 7. Chondrite-normalized REE patterns .Normalizing values are from Boynton (1985).

These intrusions have 10,000 Ga/Al ratios ranging from 1.8 to 2.3 and K_2O+Na_2O from 4.5 to 8.3, lower than typical A-type granites. In the plots (Fig. 9) of 10,000 Ga/Al vs. K_2O+Na_2O and $(K_2O+ Na_2O)/CaO$ (Whalen *et al.*, 1987), both the samples fall in the fields of I- and S-type granites. In addition, contrast to the highly siliceous S-type granites that are typically strongly peraluminous with A/CNK value much higher than 1.1(Chappell and White, 1992; 2001; Clemens *et al.*, 2011), these rocks have A/CNK values below 1.0 (Fig. 5) and the Magnetic susceptibility of Granotoide samples are more than 480×10^{-5}SI. Further-more, P_2O_5 contents range from 0.2 to 0.49 that are negatively correlated with SiO_2 (Fig. 3g) which is regarded as an important criterion for distinguishing I-type granites from S-type granites because apatite reaches saturation in metaluminous and mildly peraluminous magmas (A/CNK lower than 1.1), but is highly soluble in strongly peraluminous melts (Li *et al.*, 2007).

Thus, the Boroon Granitoide is a typical I-type, rather than an A- or S-type intrusion. In agreement with the metaluminous and I-type characteristics of Boroon granitoids, these rocks plot on the fields of the volcanic arc granites (Fig. 10), in the diagrams proposed by Pearce *et al.* (1984). According to Schandl and Gorton 2002 diagrams ,these rocks formed in active continental margins (Fig. 11). According to Sr/Y vs. Y and $(Yb)_N$ vs. $(La/Yb)_N$ in Martin 1999 and Defant and Drummond 1990 discrimination diagrams, Boroon granitoids located in classic island arc (Fig. 12a and b).

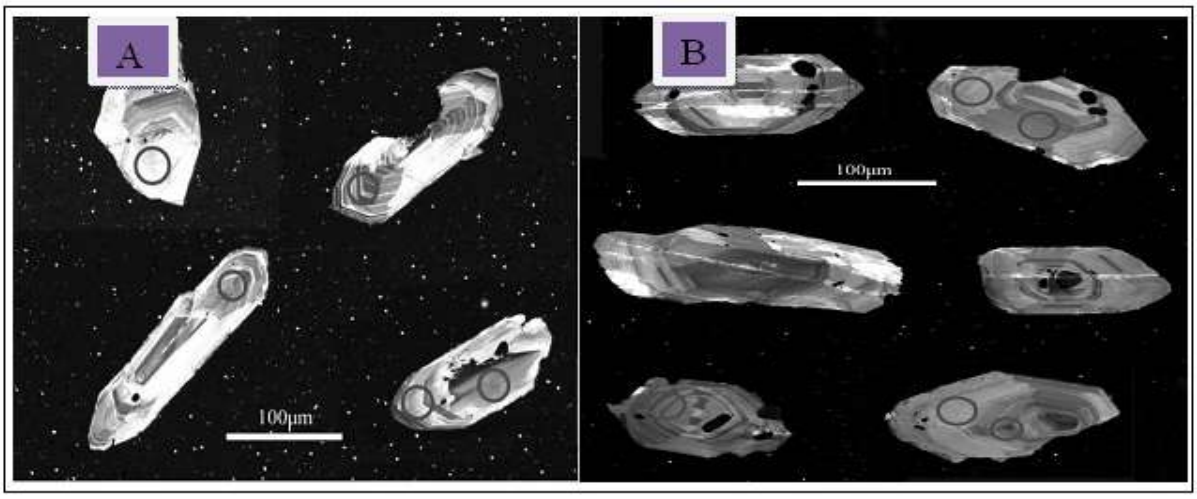

Fig. 8. Cathodoluminescence images of representative zircon grains from samples 367 (A), M15 (B). The red circles indicate the analyzed spots.

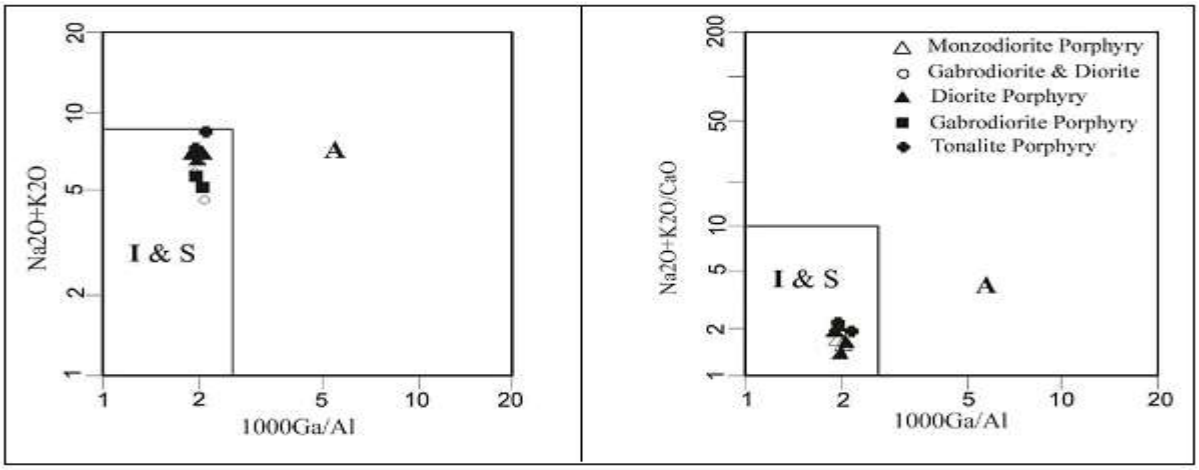

Fig. 9. Granite discrimination diagrams (Whalen *et al*. 1987).

Primitive mantle-normalized trace element spider diagrams (Sun and McDonough, 1989) display strong enrichment in large ion lithophile elements (LILE), such as Rb, Ba and Cs, and other incompatible elements that behave very similarly to LILE (Th and U). The most characteristic high field strength elements (HFSE) – e.g. Nb, Zr, Y, Ti and HREE – have, compared to LILE, clearly lower normalized values; Nb, Ti, in particular, define deep negative anomalies (Fig. 6). These features are typical of the subduction-related magmas, namely in the calc-alkaline volcanic arcs of continental active margins (e.g.: Gill, 1981; Pearce, 1983; Wilson, 1989; Walker *et al*., 2001). Their high Sr and low Nb, Ta and Ti contents are thought to be due to the absence of plagioclase and presence of Fe–Ti oxides in the residue in the source area of the parental magmas (Martin, 1999); Nb and Ta contents may also be viewed as resulting from previous depletion events in the mantle source rocks (Woodhead *et al.,* 1993; Gust *et al.,* 1997). Phosphorous also show negative anomalies in the studied samples, which may be related to apatite fractionation. Although, in general, as already described, LILE are enriched relative to HFSE, Rb and Ba display low normalized values if compared to other LILE; this decoupling of the behavior of Rb and Ba compared to other LILE may be explained by the involvement of the addition of a sediment component from the subducted slab during the compositional changes underwent by the peridotites of the source area (Borg *et al*., 1997; Leat *et al*., 2003). Rare-earth element patterns in

chondrite-normalized plots display high degrees of REE fractionation (Fig. 7), with strong LREE enrichment ($4.9 \leq La_N/Yb_N \leq 8.4$). All the studied rocks have Eu/Eu* ratios from 0.65 to 0.88. Normally, a negative Eu anomaly develops with magma differentiation due to fractional crystallization of early plagioclase (Henderson, 1984).

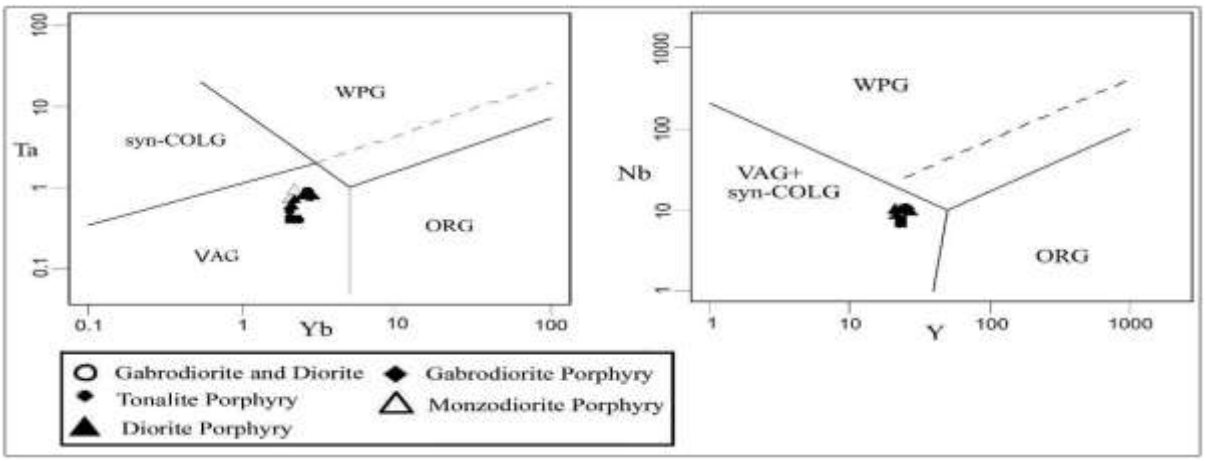

Fig. 10. Tectono-magmatic discrimination diagrams (Pearce *et al.*, 1984).

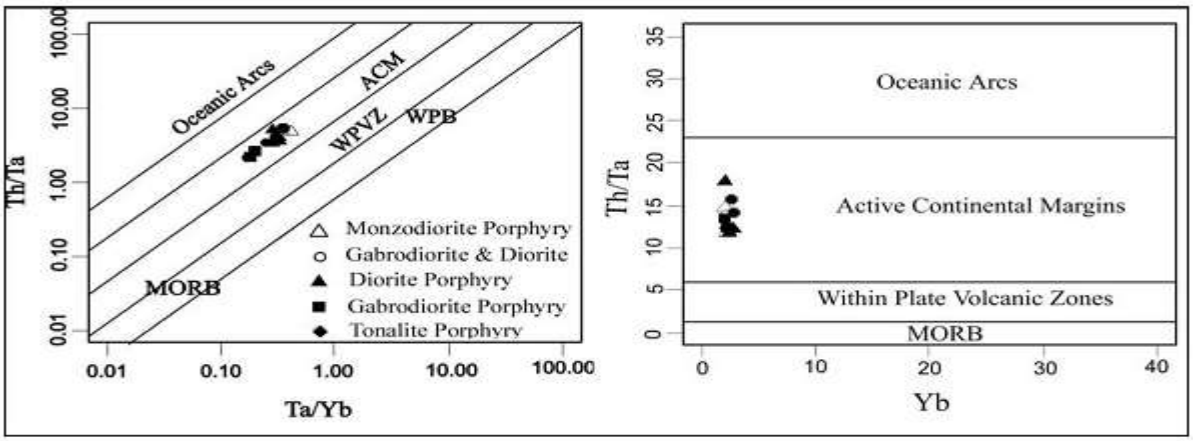

Fig. 11. Tectonomagmatic discrimination diagrams (Schandl and Gorton 2002).

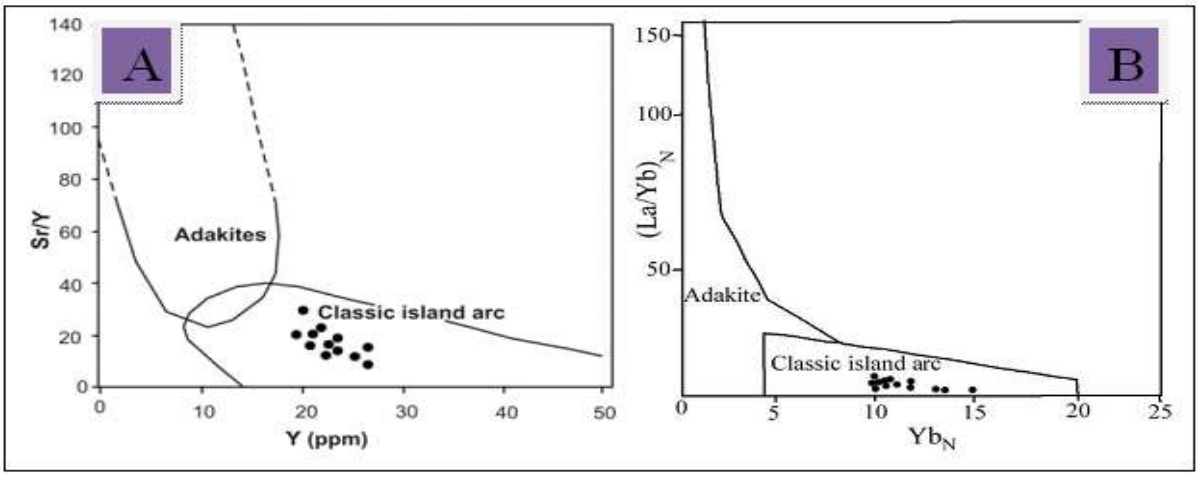

Fig. 12. A- Boroon intrusives on Y versus Sr/Y. Fields after Defant and Drummond (1990). B- Boroon intrusives on YbN versus (La/Yb)N. Fields after Martin, 1999.

Conclusion

Major element geochemistry reveals that all the studied lithologies are typically metaluminous (A/CNK ≤ 0.94) and, in addition, suggest, that they constitute a suite belonging to the high-K calc-alkaline series. Magnetite susceptibility (1485 * 10-5 SI) together with mineralogical and geochemical features shows that they belong to magnetite granitoid series (I-type). In primitive mantle-normalized trace element spiderdiagrams, the analysed samples display strong enrichment in LILE compared to HFSE ($15.5 \leq Rb_N/Y_N \leq 45.9$), accompannied by negative anomalies of Nb, Ta and Ti. REE chondrite-normalized plots show slight to moderate LREE enrichment ($4.9 \leq La_N/Lu_N \leq 8.4$) and negative Eu anomalies (Eu/Eu* ratios vary from 0.65 to 0.88. The Zircon U–Pb Geochronology show an intrusion age of 40.31 ± 0.82 Ma (M15) for the Boroon granitoids that continued to 31.88 ± 0.2 Ma (367). These granitoids display trace element features typical of the magmatism related to a subduction zone, such as LILE enrichment and marked Nb, Ta and Ti negative anomalies. Geochemical evidence shows that the Boroon intrusives belong to the magnetite series, with mineral potential for Cu–Zn (Au–Ag–Pb). Isotope geochemistry shows that the studied rocks are co-genetic and should be related to each other mainly by magmatic differentiation processes, such as fractional crystallization. Therefore, the high K_2O contents should result from assimilation of crustal materials rather than from the mantle source geochemistry. Despite the fact that no primitive melt is directly represented by any of the studied rocks, some hypotheses on the processes involving the mantle source may be put forward: The parental magmas probably derived from partial melting of metasomatized peridotite in a supra-subduction mantle wedge; during the melting event, phlogopite breakdown should have contributed to some of the most important geochemical fingerprints of the suite; garnet and amphibole possibly remained as residual phases in the source. This study provides new evidence for subduction beneath the Lut Block during the Tertiary. A spatial and temporal relationship between tectono-magmatic cycles in the eastern Iran arc and porphyry Cu–(Mo–Au) formation has been recognized. Cu–Au porphyry deposits of the Lut Block seem to be related to an immature arc geotectonic setting during the middle Eocene, while Mo-bearing porphyry-type deposits correspond to a more advanced stage of arc evolution and probably to crustal thickening as a result of the beginning of Afghan and Lut plate collision during Oligocene.

References

Aghanabati S. 1383. Geology of Iran. Publications of the Geological Survey of Iran.

Porlatifi A. 1382. Geological map of Ferdows 1/100000. Publications of the Geological Survey of Iran.

Geological and mining Exploration of Iran. 1382. Geochemical Exploration in a 1: 100,000 Ferdows map.

Angiboust S, Agard P, De Hoog JCM, Omrani J, Plunder A. 2013. Insights on deep. accretionary subduction processes from the Sistan ophiolitic“melange”(Eastern Iran). Lithos 156–159, 139–158.

Arjmandzadeh R, Santos SA. 2013. Sr–Nd isotope geochemistry and tectonomagmatic setting of the Dehsalm Cu–Mo porphyry mineralizing intrusives from Lut Block. eastern Iran. International Journal of Earth Sciences, (GeolRundsch) **103,** 123-140 p.

Borg LE, Clynne MA, Bullen TD. 1997. The variable role of slab-derived fluids in the generation of a suite of primitive calc-alkaline lavas from the southernmost Cascades. California. The Canadian Mineralogist **35.** 425–452.

Boynton WV. 1985. Cosmochemistry of the rare earth elements: meteorite studies. in rare earth element geochemistry. Elsevier. Amsterdam.

Berberian M, King GC. 1981. Towards a paleogeography and tectonic evolution of Iran. Canadian Journal of Earth Sciences **(18),** 210–265.

Babazadeh SA, De Wever P. 2004. Early Cretaceous radiolarian assemblages from radiolarites in the Sistan Suture (eastern Iran). Geodiversitas **26.** 185–206.

Camp VE, Griffis RJ. 1982. Character. genesis and tectonic setting of igneous rocks in the Sistan suture zone. eastern Iran. Lithos **15.** 221–239.

Chappell BW, White AJR. 1992. I- and S- type granites in the Lachlan Fold Belt. Transactions of the Royal Society of Edinburg. Earth Science **(83),** 1-26.

Chappell BW, White AJR. 2001. Two contrasting granite type: 25 years later. Australian Journal of Earth Science **(48),** 489-499.

Chen B. 2009. Petrogenesis of mafic enclaves from the north Taihang Yanshanian intermediate to felsic plutons: evidence from petrological. Geochemical. and zircon Hf–O isotopic data. Science in China Series D: Earth Sciences **52,** 1331–1344.

Clemens JD, Stevens G, Farina F. 2011. The enigmatic sources of I-type granites: the peritectic connexion. Lithos **126 (3–4),** 174–181.

Defant MJ, Drummond MS. 1990. Derivation of some modern arc magmas by melting of young subducted lithosphere. Nature **(347),** 662–665.

Dela Roche H, Leterrier J, Grande Claude P, Marchal M. 1980. A classification of volcanic and plutonic rocks using R1-R2 diagrams and major element analyses its relationships and current nomenclature. Chemical Geology **(29),** 183–210.

De Paolo DJ. 1981. Trace element and isotopic effects of combined wallrock assimilation and fractional crystallisation. Earth Planet. Sci. Lett. **53.** 189-202.

Eby GN, Woolley AR, Din V, Platt G. 1998. Geochemistry and petrogenesis of nepheline syenite: Kasungu–Chipala Ilombaand Ulindi nepheline syenite in-trusions. North Nyasa Alkaline Province.Malawi. Journal of Petrology **39.** 1405–1424.

Faure G, Mensing TM. 2005. Isotopes: Principles and Applications. John Wiley and Sons. New Jersey.

Gust DA, Arculus RA, Kersting AB. 1997. Aspects of magma sources and processes in the Honshu arc. The Canadian Mineralogist 35. 347–365.

Gill JB. 1981. Orogenic andesites and plate tectonics. Springer. New York.

Griffis AR, Magries H, Abedian N, Behrozi A. 1991. Explanatory text of Dehsalm (Chahvak). Geological Quadrangle Map 1:250000. No. K6. Geological Survey of Iran. Tehran.

Hanchar JM, Hoskin PWO. 2003. Zircon. Reviews in Mineralogy and Geochemistry 53. 1–500.

Henderson P. 1984. Rare Earth Element Geochemistry. Elsevier. Amsterdam. 510 p..

Ishihara S. 1977. The magnetite- series and ilmenite-series granitic rocks. Mining Geology **(27),** 293-305.

Ishihara S. 1981. The granitoid series and mineralization. Economic Geology **(75),** 458-484.